Optics Communications 285 (2012) 347–351

Contents lists available at SciVerse ScienceDirect

Optics Communications

journal homepage: www.elsevier.com/locate/optcom

Phase-matched generation of high-order continuous-wave coherent Raman sidebands

Shin-ichi Zaitsu [a,b,*], Totaro Imasaka [a,c]

[a] Graduate School of Engineering, Kyushu University, 744 Motooka, Nishi-ku, Fukuoka, 819-0395, Japan
[b] PRESTO, Japan Science and Technology Agency, 4-1-8 Honcho Kawaguchi, Saitama, 332-0012, Japan
[c] Center for Future Chemistry, Kyushu University, 744 Motooka, Nishi-ku, Fukuoka, 819-0395, Japan

ARTICLE INFO

Article history:
Received 6 July 2011
Received in revised form 17 September 2011
Accepted 19 September 2011
Available online 6 October 2011

Keywords:
Nonlinear optics
Four-wave mixing
Stimulated Raman scattering
Optical cavity

ABSTRACT

We demonstrate the generation of continuous-wave (cw) Raman sidebands through phase-matched four-wave mixing (FWM) in molecular hydrogen. The phase-matching conditions of the intracavity FWM driven in our dispersion-compensated high-finesse cavity are satisfied over a 52.8 THz-wide frequency range (763.9–883.6 nm). This leads to the generation of high-order anti-Stokes emission. The cw Raman sidebands have sufficient bandwidth to allow the synthesis of a train of optical pulses with a duration of 13 fs at a repetition rate of 17.6 THz under phase-locked conditions.

1. Introduction

Coherent Raman scattering, which arises from molecular motion that is driven coherently through stimulated excitation, has been widely investigated. It is a practical tool used in a variety of research fields, including laser engineering, spectroscopy and microscopy [1–4]. One promising application of this versatile nonlinear optical effect is the generation of broadband coherent Raman sidebands [5–8]. The adiabatic excitation of molecular coherence using two-color nanosecond lasers gave rise to extremely broadband Raman sidebands that spanned more than one octave within the optical spectrum [5,6]. These sidebands were used to create a train of optical pulses with a duration of less than one cycle of the electromagnetic field [7] and an arbitrary waveform [8].

In previous studies, high-energy pulsed lasers were used to excite strong coherent motion in molecules, which converts the fundamental frequency of the laser beam into multiple orders of Raman sidebands [9–11]. However, low-peak-power continuous-wave (cw) lasers also have been used to produce stimulated Raman scattering (SRS) through the use of high-finesse optical cavities [12]. This technique offers a way to induce nonlinear optical interaction between coherent molecular motion and low-power cw lasers, and can serve as the basis for an optical modulator [13,14] and for a mode-locked laser [15] operating at a frequency in the terahertz region.

This cavity-enhanced technique, however, cannot be directly applied to the generation of cw Raman sidebands on the high frequency side of the fundamental, because they are generated through four-wave mixing (FWM) rather than SRS. The FWM process requires phase-matching between the sidebands during the interaction in the nonlinear optical medium. Unfortunately, dispersion, which is inevitably present in the material over the entire optical spectrum, distorts the phase relationship between the sidebands. This prevents phase-matched FWM in the optical cavity.

To overcome this difficulty, approaches using hollow-core photonic crystal fibers have been used in the pulsed laser regime [16,17]. In the cw laser regime, negative-dispersion cavity mirrors to compensate for the dispersion of the intracavity medium [18] and high-power pumping of a dilute gas to extend the coherence length of the FWM [14] have been proposed and used for the generation of cw anti-Stokes emission. Although the high-order phase-matched cw Raman sidebands are essential for the synthesis of an optical waveform, they have not yet been obtained in the cw regime. This is because of the limitations imposed on the frequency range of the high-finesse and dispersion-compensated optical cavity.

In this letter, we demonstrate the generation of high-order cw Raman sidebands using Raman-resonant FWM in a broadband dispersion-compensated high-finesse optical cavity. The phase-matched interaction between hydrogen molecules and the Raman sidebands in the optical cavity provides five single-frequency lines, spanning from the second anti-Stokes line (763.9 nm) to the second Stokes line (930.9 nm).

2. Design of an optical cavity and experimental setup

In the ideal case, i.e., without pump depletion or back-conversion from anti-Stokes photons to Stokes photons, the efficiency of the

* Corresponding author at: Graduate School of Engineering, Kyushu University, 744 Motooka, Nishi-ku, Fukuoka, 819-0395, Japan.
E-mail address: s-zaitsu@cstf.kyushu-u.ac.jp (S. Zaitsu).

0030-4018/$ – see front matter © 2011 Elsevier B.V. All rights reserved.
doi:10.1016/j.optcom.2011.09.054

FWM process is maximized under phase-matched conditions, i.e., when the phase-mismatch, Δk, is equal to zero. Δk is determined by the Raman frequency shift, Ω, and the even-order dispersion coefficients of the Raman-active medium, β_{2m}:

$$\Delta k = \sum_{n=2m}^{\infty} \frac{2}{n!}\beta_n \Omega^n. \quad (1)$$

For FWM in an optical cavity, the effect of the dispersion is given by the sum of the contributions from the medium in the cavity and from the cavity mirrors. Our dispersion-compensated optical cavity was a key component for the generation of cw Raman sidebands through intracavity FWM. It consisted of a pair of plano-concave mirrors with a curvature of 25 cm, spaced 8 cm apart, and installed in a chamber filled with as much as 1 MPa of hydrogen for use as the Raman-active medium. Here, the cavity mirrors are designed to have negative dispersive properties, and the dash-dotted curve shown in Fig. 1(a) represents the designed value of the group delay (GD) after one bounce from a cavity mirror. The GD of the gas-phase hydrogen [19] at a pressure of 820 kPa (dashed curve) and the total GD calculated from the sum of these GDs (solid curve) are also shown in the figure. The negative dispersion of the cavity mirror compensates for the positive dispersion of the medium in the cavity. This leads to a variation of less than ± 0.4 fs in total GD over the wavelength range from 750 to 950 nm. The mirrors are also designed to have a reflectivity of more than 99.97% over the same wavelength range. The transmittance spectrum, which was provided by the manufacturer, is shown in Fig. 1(b). This highly-reflective range with negative dispersion is approximately twice as large as that of previously reported mirrors [18,20]. A single-frequency wavelength-tunable cw laser (MBR110, Coherent, Santa Clara, CA, USA) was used as the pump beam for the intracavity FWM. The pump beam frequency was set to 839.2 nm, which is nearly in the center of the dispersion-compensated region of the cavity. The pump beam, which has a power of ~1.5 W, was coupled into the hydrogen-filled cavity. The power and the spectrum of the output beam were measured simultaneously using a silicon photodiode power sensor (OP2, Coherent) and a multichannel spectrometer (HR4000, Ocean Optics, Dunedin, FL, USA), respectively. The maximum power of the output beam was ~50 mW.

3. Results and discussions

In the first experiment, we measured the output beam spectra while changing the intracavity hydrogen pressure from 200 kPa to 1 MPa in a series of coarse steps. The typical output spectrum measured at an intracavity pressure of 626.8 kPa is shown in Fig. 2(a). In addition to the emission line of the pump laser (ω_0: 839.2 nm), lines at 882.6 nm and 930.9 nm were observed. These newly generated lines can be assigned to the first Stokes line (ω_1) and the second Stokes line (ω_2), corresponding to the rotational transition of *ortho* hydrogen ($S_0(1)$: $J=1 \rightarrow J=3$, $\Omega=17.6$ THz). Although we observed a slight difference in the ratios between the intensities of the three lines during the change in pressure, we did not observe any other emission lines while tuning over the entire pressure range by coarsely changing the intracavity hydrogen pressure. Because SRS automatically fulfills the phase-matching condition for the growth of the Stokes beam [21], the component of the dispersion that depends directly on the pressure does not affect the SRS process. Therefore, it can be seen that ω_1 and ω_2 observed here arose from cascaded SRS, and FWM did not contribute to these lines, because it requires the phase-matching condition to be satisfied.

In the next experiment, we measured the spectra while fine-tuning the intracavity pressure near 800 kPa. The emission line at a wavelength of 799.8 nm, which corresponds to the first anti-Stokes line (ω_{-1}), was observed at a pressure of 818.1 kPa (see Fig. 2(b)). An anti-Stokes photon can be generated through FWM that involves two photons at ω_0 and one photon at ω_1 (see the inset of Fig. 2(b)). In contrast to SRS, the gain for FWM is critically dependent on the phase-matching between the interacting lightwaves [18]. The generation of ω_{-1} observed here indicates that the compensation of the intracavity dispersion at the pressure of 818.1 kPa gave rise to phase-matched conditions for FWM in the optical cavity. This led to enhancement of the intensity of ω_{-1} in the output beam.

The generation of a second anti-Stokes emission line (ω_{-2}: 763.9 nm) in addition to ω_{-1} was observed when the intracavity pressure was slightly increased (Fig. 3(a)). The intensity of ω_{-2} was the largest at a pressure of 828.8 kPa. For the generation of ω_{-2}, three possible pathways for the frequency conversion process are shown in Fig. 3(b)–(d). To determine which pathways contributed to the generation of ω_{-2}, we measured the thresholds for the generation of the Raman sidebands. Fig. 3(e) shows the evolution of the sideband intensities as a function of the total output power. The thresholds for the generation of ω_1, ω_{-1}, and ω_{-2} were all 10 mW, but the threshold for ω_2 (24 mW) was larger than those of the other sidebands. The threshold for the SRS process is determined by the ratio between the gain and the cavity loss [22]. However, in FWM, the threshold for anti-Stokes emission is identical to that for Stokes emission because FWM is a parametric process. This means that it leads to the simultaneous generation of one Stokes photon and one anti-Stokes photon from two pump

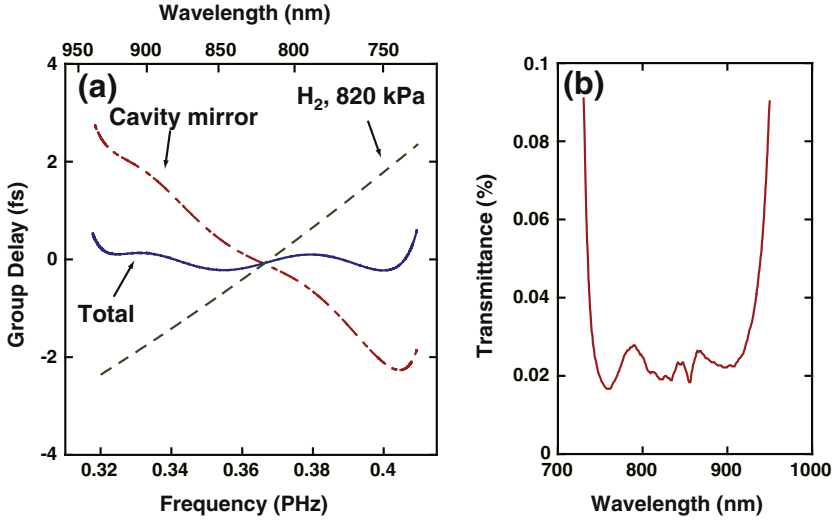

Fig. 1. (a) GDs from a single bounce from the surface of the cavity mirror (designed value, dash-dotted line), H_2 gas at a pressure of 820 kPa (dashed line), and the sum of these GDs (solid line). (b) Transmittance of the cavity mirror.

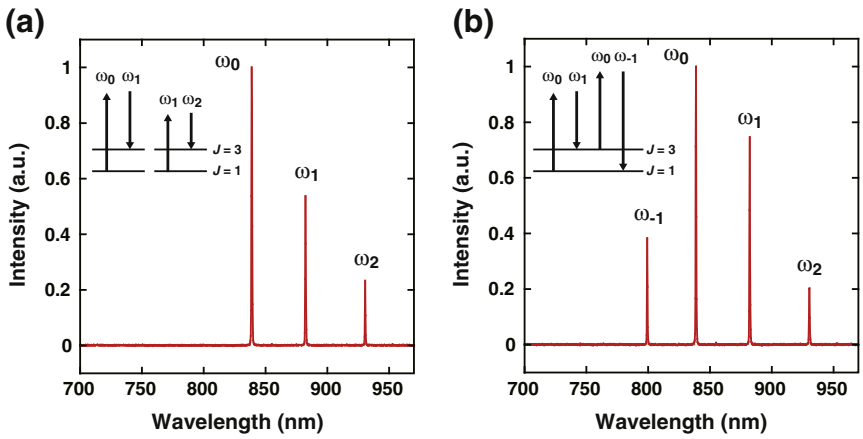

Fig. 2. (a) Spectrum of the output beam measured at H_2 pressure of 626.8 kPa. (b) Spectrum measured at H_2 pressure of 818.1 kPa, which led to generation of ω_{-1} from phase-matched FWM that involves two photons at ω_0 and one photon at ω_1.

photons. Therefore, the coincidence of the thresholds for the generation of ω_1 and ω_{-2} shown in Fig. 3(e) suggests that the pathway shown in Fig. 3(c) was not valid for the generation mechanism of ω_2 in this result, and that ω_2 was generated through cascaded SRS using ω_1 as a pump photon. Fig. 3(e) shows a decrease in the growth of the intensity of ω_{-1} at the total output power where the intensity of ω_{-2} grows significantly (see the intensity variation around 24 mW). This implies that the pathway shown in Fig. 3(b) was mainly responsible for the generation of ω_{-2} because Fig. 3(b) involves the generation of an ω_{-2} photon at the cost of an ω_{-1} photon. Theoretical models that describe the evolution of the intracavity powers of high-order Stokes and anti-Stokes emissions arising from both SRS and FWM processes will be helpful to determine which of the pathways shown in Fig. 3(b) and (d) contribute to the generation of ω_{-2}.

We have studied the efficiencies of this frequency conversion process from the application viewpoint. The total output power was ~30 mW, which indicated that 2% of the input beam was coupled out of the Raman cavity. 40% of the output power was distributed in the Raman sidebands, which means that the total conversion efficiency was ~0.8%. The total conversion efficiency can be significantly improved by reducing the optical losses of the cavity mirrors and optimizing the input power level. Redesign of the transmission spectrum of the cavity mirrors will also lead to a modified power distribution for each Raman sideband.

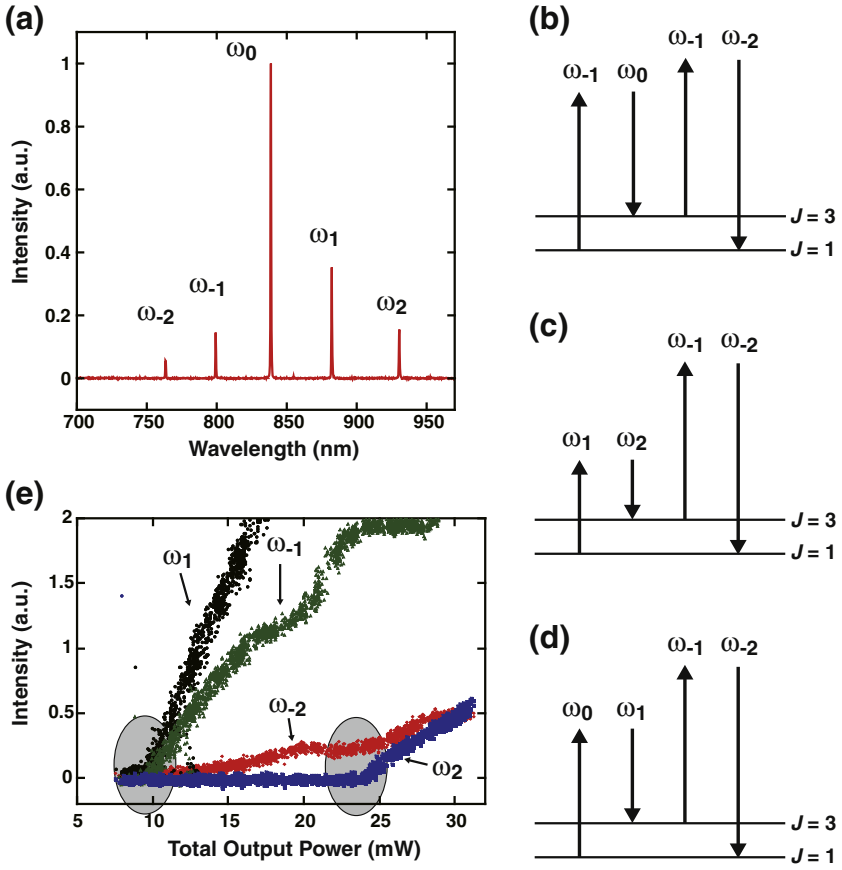

Fig. 3. (a) Spectrum measured at H_2 pressure of 828.8 kPa. A line corresponding to ω_{-2} can be seen. (b)–(d) Possible pathways for the generation of ω_{-2} through FWM. (e) Evolution of the Raman sidebands as a function of total output power with ω_{-2} present.

The dependence of the intracavity FWM on the intracavity dispersion can be explained by the rearrangement of the longitudinal modes of the Raman cavity. The separation frequencies between adjacent longitudinal modes of an optical cavity filled with a medium increase with an increase in the optical frequency because of the positive group delay dispersion (GDD) of the medium in the cavity [23]. Fig. 4 shows a series of longitudinal modes of the optical cavity and the SRS gain curves against the different intracavity dispersion conditions when the pumping frequency is ω_0. The SRS gain has a bandwidth due to inhomogeneous broadening (~1 GHz at 1 MPa of hydrogen molecules [24]), which allows us to generate ω_1 and ω_2 when the longitudinal modes are separated by uneven frequency intervals, as shown in Fig. 4(a). This is the reason why the spectrum shown in Fig. 2(a) was observed independently of the intracavity dispersion. On the other hand, the FWM gain is determined by the phase-matching conditions between the intracavity emissions. The FWM gain for the generation of ω_{-1} presents at a frequency that is separated from ω_0 by $\Omega=\omega_0-\omega_1$ (see Fig. 4(b)), which resulted from the energy conservation low in the FWM process, i.e., $2\omega_0=\omega_1+\omega_{-1}$. The compensation of the intracavity dispersion rearranges the longitudinal modes responsible for the generation of the sidebands so that they are separated by a constant interval. Overlapping of one of the longitudinal modes with the frequency of $\omega_0+\Omega$ allowed ω_{-1} to be enhanced through the phase-matched FWM, leading to the spectrum shown in Fig. 2(b). In the same manner, when the longitudinal modes responsible for the FWM are spaced at a constant interval from ω_1 to ω_{-2} (Fig. 4(c)), ω_{-2} is generated through the phase-matched FWM, giving rise to the spectrum shown in Fig. 3(a). From Fig. 2(b), it can be seen that because ω_2 was generated through cascaded SRS rather than phase-matched FWM, the frequency range for the phase-matched FWM can be calculated to be 35.2 THz, which is the span from ω_1 to ω_{-1}. However, the frequency range for the phase-matched FWM, which is shown in Fig. 3(a), was extended to 52.8 THz because of the generation of ω_{-2}.

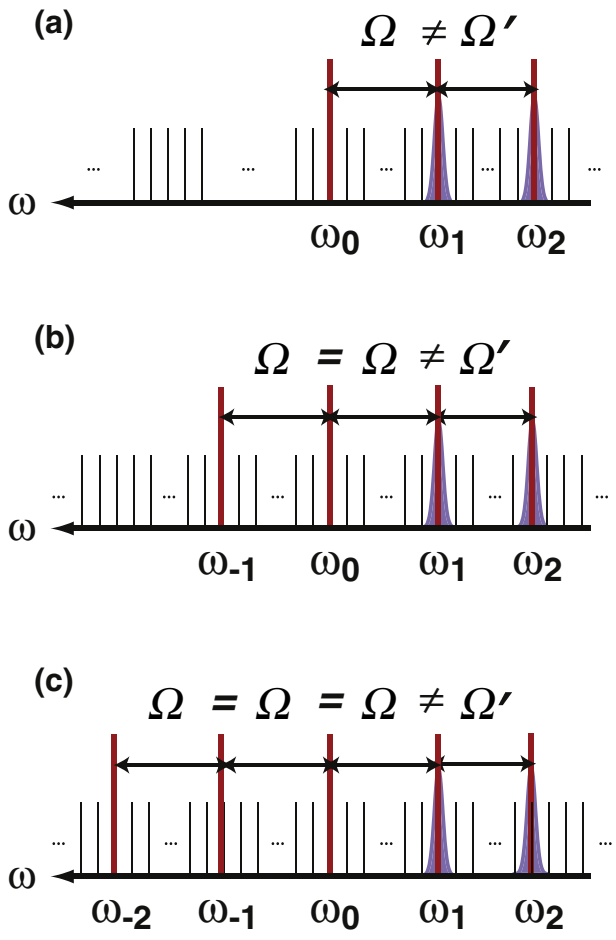

Fig. 4. The relationship between the longitudinal modes of a medium-filled optical cavity and the gain curve for SRS and FWM. (a) The medium in the optical cavity has a positive dispersion. (b) The negative dispersion of the cavity mirrors is compensated for by the medium dispersion in the frequency range from ω_{-1} to ω_1. (c) The intracavity dispersion is compensated over the frequency range from ω_{-2} to ω_1.

Unfortunately, the frequency dependence of the GD of the negative dispersive mirrors used in this experiment has a ripple, which is typical of this type of mirror. This contributes to high-order dispersion, which is difficult to compensate for by using only the intracavity pressure. Even after compensating for the GDD of the optical cavity, the residual high-order dispersion prevents the simultaneous generation of ω_2 and other emission lines through phase-matched FWM. One possible way to suppress the dispersion ripple is the use of a pair of double-chirped mirrors, which modulate the GD using opposite phases. This broadens the frequency range of phase-matching for intracavity FWM. When the phase-matching conditions for FWM for the five emission lines from ω_2 to ω_{-2} are satisfied, it will enable the generation of an equally-spaced multifrequency cw laser. The laser output will consist of single-frequency emission lines with a constant separation of 17.6 THz over a 70.4 THz-wide frequency range. The phase-locked multiple single-frequency lines allow the synthesis of an optical pulse train in the time domain. Because the mutual phase coherence between the cw Raman sidebands had already been verified experimentally in previous literature [14], our lasers are expected to form a repeating train of optical pulses with a duration of 13 fs and an interval of 57 fs. Thus, this phase-matched intracavity FWM process with a cw laser has the potential to produce a novel optical modulator and a mode-locked laser that can operate at a repetition frequency of more than 10 THz.

4. Conclusions

We have demonstrated the generation of broadband (70.4 THz) cw Raman sidebands that consist of five single-frequency emission lines separated by frequency intervals of 17.6 THz. These emission lines are generated from phase-matched Raman-resonant FWM induced in a hydrogen-filled high-finesse optical cavity with a tunable intracavity dispersion. The observation of the thresholds for the emission lines revealed that the high-order Stokes and anti-Stokes lines were generated through SRS and phase-matched FWM, respectively. The frequency range for the phase-matching of the FWM was found to be 52.8 THz wide (763.9–883.6 nm). The synthesis of the cw Raman sidebands generated through the phase-matched FWM has the potential to generate an optical pulse train and form arbitrarily-shaped optical waveforms. This approach can be easily extended to other Raman-active gases, e.g., *para*-hydrogen, deuterium, methane, etc., which will lead to a wide variety of separation frequencies between the sidebands and will cover a wide range of repetition frequencies for synthesized optical pulse trains.

Acknowledgments

This research was supported through the PRESTO program from the Japan Science and Technology Agency (JST), Grants-in-Aid for Scientific Research and the Global COE Program “Science for Future Molecular Systems” from the Ministry of Education, Culture, Science, Sports and Technology of Japan.

References

[1] S.A.J. Druet, J.P.E. Taran, Progress Quantitative Electrical 7 (1981) 1.
[2] K. Kneipp, H. Kneipp, Applied Spectroscopy 60 (2006) 322A.
[3] M. Müller, A. Zumbusch, ChemPhysChem 8 (2007) 2156.
[4] N. Vermeulen, C. Debaes, H. Thienpont, Laser & Photonics Reviews 5 (2010) 656.

[5] T. Imasaka, S. Kawasaki, N. Ishibashi, Applied Physics B 49 (1989) 389.
[6] A.V. Sokolov, D.R. Walker, D.D. Yavus, G.Y. Yin, S.E. Harris, Physical Review Letters 85 (2000) 562.
[7] M.Y. Shverdin, D.R. Walker, D.D. Yavuz, G.Y. Yin, S.E. Harris, Physical Review Letters 94 (2005) 033904.
[8] H. Chan, Z. Hsieh, W. Liang, A. Kung, C. Lee, C. Lai, R. Pan, L. Peng, Science 331 (2011) 1165.
[9] R.A. Bartels, T.C. Weinacht, N. Wagner, M. Baertschy, C.H. Greene, M.M. Murnane, H.C. Kapteyn, Physical Review Letters 88 (2002) 013903.
[10] N. Zhavoronkov, G. Korn, Physical Review Letters 88 (2002) 203901.
[11] Y. Kida, S. Zaitsu, T. Imasaka, Optics Express 16 (2008) 13492.
[12] J.K. Brasseur, K.S. Repasky, J.L. Carlsten, Optics Letters 23 (1998) 367.
[13] K. Ihara, C. Eshima, S. Zaitsu, S. Kamitomo, K. Shinzen, Y. Hirakawa, T. Imasaka, Applied Physics Letters 88 (2006) 074101.
[14] J.T. Green, J.J. Weber, D.D. Yavuz, Physical Review A 82 (2010) 011805(R).
[15] K. Shinzen, Y. Hirakawa, T. Imasaka, Physical Review Letters 87 (2001) 223901.
[16] A.B. Fedotov, S.O. Konorov, V.P. Mitrokhin, E.E. Serebryannikov, A.M. Zheltikov, Physical Review A 70 (2004) 045802.
[17] A. Nazarkin, A. Abdolvand, P.St.J. Russell, Physical Review A 79 (2009) 031805(R).
[18] S. Zaitsu, H. Izaki, T. Imasaka, Physical Review Letters 100 (2008) 073901.
[19] E.R. Peck, S. Huang, Journal of Optics Society American 67 (1977) 1550.
[20] This improvement was contributed by the sophisticated design of the mirrors by the manufacture (Layertec GmbH, Mellingen, Germany).
[21] R.W. Boyd, Academic Press, 2003, p. 462.
[22] K.S. Repasky, J.K. Brasseur, L. Meng, J.L. Carlsten, Journal of Optics Society American 15 (1998) 1667.
[23] P.A. Siegman, University Science Books, 1986, p. 437.
[24] G.C. Herring, Mark J. Dyer, William K. Bischel, Physical Review A 34 (1986) 1944.